Environmental Research 233 (2023) 116434

Contents lists available at ScienceDirect

Environmental Research

journal homepage: www.elsevier.com/locate/envres

A three-dimensional perspective of phosphorus retention across a field-buffer strip transition

David Ramler [a,*], Erich Inselsbacher [b], Peter Strauss [a]

[a] Institute for Land and Water Management Research, Federal Agency for Water Management, Pollnbergstraße 1, 3252, Petzenkirchen, Austria
[b] Department of Forest- and Soil Sciences, Institute of Soil Research, University of Natural Resources and Life Sciences Vienna, Peter-Jordan-Strasse 82, 1190, Vienna, Austria

ARTICLE INFO

Keywords:
Vegetated filter strip
Riparian buffer strip
Degree of phosphorus saturation (DPS)
Phosphorus sorption index (PSI)
Surface water protection
Soil core sampling

ABSTRACT

Vegetated filter strips (VFS) act as buffer zones between fields and water bodies that are supposed to retain incoming runoff, sediment, and nutrients. The factors that govern nutrient retention and cycling in VFS are complex and act in all three dimensions. A key element that determines VFS effectivity is flow type, e.g., sheet vs. concentrated flow. These aspects are, however, often insufficiently accounted for in VFS research and design recommendations. In this study, we attempt to tackle these shortcomings by examining the nutrient distribution in detail at two field-VFS transitions, applying a three-dimensional sampling array together with extensive laboratory analyses. Concentrated runoff was the dominant type we found and we argue that flow convergence is the norm rather than the exception. Further complicating this issue is that entry locations of runoff may vary, calling for more sophisticated sampling designs. Overall trends were similar across the analyzed nutrient fractions (different K- and P-pools) and there were distinct trends of decreasing nutrients along the longitudinal (from the field to the VFS) and vertical planes. The horizontal plane (from outside to inside the area of concentrated flow) showed mostly inconclusive or U-shaped gradients. Both sites were similar and close to each other, nevertheless, there were significant differences that affected nutrient retention in the VFS which were linked to site-specific factors. The spatial extent (i.e., width) is often considered the main variable in VFS designs. However, other VFS traits such as vegetation type and structure, as well as external factors such as field topography and the severity of erosive events are equally important and should be attributed more significance.

1. Introduction

Eutrophication remains a major problem for water bodies in Europe. Phosphorus (P) is one of the most important drivers of nutrient pollution, as it is commonly the limiting factor in aquatic systems (Schindler et al., 2016; Ulén et al., 2007). After considerable success during the last decades in purifying wastewater, major P sources remain inputs from agricultural areas via runoff and erosion (Stoate et al., 2009). In-field conservation measures and prevention of a build-up of nutrients in the first place are considered the most effective mitigation actions. However, these may not be sufficient (e.g., during intense rainfall events) or are not implemented because of other reasons such as high costs or low acceptance among farmers (Bailey et al., 2013; Hösl and Strauss, 2016; Schoumans et al., 2014). Often used and recommended alternatives are vegetated filter strips (VFS) between fields and water bodies (Carstensen et al., 2020; Prosser et al., 2020). These act as buffer zones that are supposed to slow down runoff and promote infiltration and sedimentation processes, leading to a retention of nutrients within the VFS. Thereby, the effectiveness of VFS largely depend on different factors such as buffer width, slope, runoff intensity, soil composition and plant community (reviewed by Prosser et al., 2020). Although there is an increasing understanding of nutrient pathways and the complex biogeochemical processes within soils, these are often not adequately addressed in research on VFS, which is, thus, partly lagging behind the latest scientific developments (Ramler et al., 2022; Weihrauch, 2019). Many VFS performance or monitoring studies focus only on buffer width and apply one-dimensional sampling designs (Prosser et al., 2020). However, the whole soil volume takes part in nutrient retention and cycling (Weihrauch, 2019). Infiltration, promoted by vegetation and further enhanced by high organismal activity, is a key function of VFS (Colloff et al., 2010; Prosser et al., 2020). Thus, the concept of VFS calls for a three-dimensional view. Another common assumption in

* Corresponding author.
E-mail address: david.ramler@baw.at (D. Ramler).

https://doi.org/10.1016/j.envres.2023.116434
Received 24 February 2023; Received in revised form 15 June 2023; Accepted 15 June 2023
Available online 19 June 2023

mathematical models and VFS design recommendations provided by agri-environmental authorities is a uniform sheet flow from the field and through the VFS. In reality, it is much more probable that VFS receive field runoff in concentrated form, e.g., due to topography, tillage, slope, or other factors that lead to flow convergence. This substantially impacts the VFS retention efficacy (Dosskey et al., 2002; Miller et al., 2016; Pankau et al., 2012). Despite this knowledge, most research on VFS retention effectivity is plot studies that apply uniform sheet flow. Consequently, many VFS design recommendations—often built upon these studies—neglect the effect of concentrated flow.

Ideally, VFS are designed so that nutrient inputs and removal (i.e., via harvesting the vegetation) are in a long-term equilibrium that prevents saturation of the VFS soil. In the EU, P loss due to water erosion varies from 0.1 to 2 kg ha^{-1} a^{-1} (Alewell et al., 2020). For a sustainable, long-term effective retention and offset of P, this amount has to be matched with the extent of the VFS and how much P can be removed by harvesting, typically ranging between 10 and 20 kg ha^{-1} a^{-1} (Hille et al., 2019). If this is not the case, VFS will inevitably become nutrient sources at some time. Substantial amounts of P may already leach from soils even if they are not fully saturated (Djodjic et al., 2004; Roberts et al., 2012; 2020). Indices such as the degree of P saturation (DPS) or the P sorption index (PSI) are viable tools to directly or indirectly assess and monitor the saturation level and P leaching probability of VFS soils (Hughes et al., 2000; Wang et al., 2016). Both indices are, however, rarely applied outside of academia, as their calculation requires specific chemical analyses which are not as widespread as other, simpler proxies for the P status in the soil used by practitioners (e.g., soil test P).

Although VFS are considered best-practice measures against diffuse pollution and nutrient losses, research has revealed a wide range of efficiencies from 100% retention to even a net release of nutrients (Carstensen et al., 2020; Hoffmann et al., 2009). Besides the inherent heterogeneity of soils in general and the multitude of contributing factors, inadequate sampling designs account for some of the inconsistencies in VFS performance or at least hinder a thorough examination of nutrient pathways (Prosser et al., 2020; Stutter et al., 2021). Therefore, research on VFS is strongly advised to apply sampling designs that match the complexity of the studied system. However, extensive field sampling and laboratory analyses are costly, making it necessary to find compromises between sufficiently elaborate sampling and limited resources.

Finally, another essential aspect of VFS studies relates to which nutrients are determined during laboratory analysis. For example, to analyze different P pools along the continuum of solubility and bioavailability, a range of weak to strong extractants (e.g., from water to hydrofluoric acid) are used (Weihrauch and Opp, 2018). To get a holistic overview of P dynamics in soils it is advisable to include more than one P fraction in VFS studies. On the other hand, the choice of the extractant also depends on the research question, and it is likely that different nutrient pools are correlated.

In this study, we attempt to tackle these often-encountered shortcomings of VFS studies by examining the nutrient retention at two field-VFS transitions, applying a three-dimensional sampling array together with extensive laboratory analyses. We aimed to answer the following research questions: What is the necessary spatial extent of a sampling array to appropriately depict the nutrient distribution of VFS, especially under the condition of concentrated runoff? What gradients of soil P parameters are found along all three dimensions? Specifically, we hypothesized that 1) P concentrations in the soil increase along the (concentrated) runoff flow path until the field edge due to accumulation and then decrease again due to infiltration and deposition in the VFS. 2) P concentrations are highest in the middle of the flow path and decrease laterally; i.e., transects inside the flow path have higher P concentrations compared to transects outside. 3) P concentrations are highest at the soil surface but elevated in subsurface layers along the flow path (following Sheppard et al., 2006).

2. Material & methods

2.1. Site description, experimental setup, and soil sampling

The two sampling sites ME01 and ME07 are located in the hilly landscape of the pre-alpine region in the district of Melk, Lower Austria, Austria (Fig. 1). At both sites, a medium-sized, low-sloping vegetated filter strip (VFS) was set up at the foot of a larger field with a pronounced inclination (Table 1). Both VFS were implemented at least 17 years before the survey. Fields were cultivated with maize during the sampling year, the primary crop in a rotation with wheat, barley, and others (Table A1). Fields were ploughed and fertilized with pig manure and mineral fertilizers following typical fertilization practices as indicated in the Austrian guide for good agricultural practices (Baumgarten, 2022). The VFS were not managed except being mowed two to three times a year. Sites were chosen based on a GIS-aided pre-selection and visual observation of substantial runoff and erosion from the fields after heavy rainfall events in the summer of 2020 (Figs. A1, A2). Due to local topography (thalwegs) and flow convergence, the fields exhibited multiple flow pathways through which runoff and sediment entered the VFS (i.e, sub-catchments). At each site, we placed the sampling grid along the flow pathway with the highest erosion.

The sampling arrays had an extent of 10 × 10 m and comprised five longitudinal transects (*A-E*; perpendicular to the field-VFS border), eight horizontal transects (*T1-T8*; parallel to the field-VFS border), and five vertical transects (i.e., depth classes), resulting in a total of 200 samples per site and a three-dimensional representation of the field and VFS soil (Fig. 2). Transect *C* was placed at the middle of the observed sediment deposition fan, which should correspond to the center of the flow path. Transect *T4* was placed along the field-VFS border. This way, physical and chemical soil gradients can be studied in all three planes: horizontally from the inside to the outside of the concentrated runoff area; longitudinally from the field into the VFS; and vertically from the surface to subsurface layers.

Soil samples were taken with exchangeable polypropylene pipes (6.8 cm inner diameter, 50 cm long) placed within a soil core sampler that was driven into the ground with the aid of an electric bell hammer or mallet and carefully removed from the soil again using a lever. The maximum sampling depth is, thus, below 50 cm, and is a compromise between sampling as deep as possible while maintaining practical and economic feasibility. The pipes were removed from the core samplers, sealed, and transported to the laboratory. Soil cores were cut at 5 cm intervals, resulting in subsamples of equal volume (ca. 180 cm^3 soil per sample). The samples from 0–5, 5–10, 10–15, 20–25, and 35–40 cm depth were then used for the analyses (Fig. 2). Sampling was carried out during October and November of 2020.

2.2. Laboratory analyses

Soil samples were air-dried at 35 °C and sieved to 2 mm. Soil texture and particle-size distributions were determined using the pipette method following international guidelines for soil monitoring (Cools and De Vos, 2020) after removing soil organic matter using 15% H_2O_2 at 70 °C.

Soil pH was determined in a 1:5 (w:v) mix of dried soil and 0.01 M $CaCl_2$. Carbonate content ($CaCO_3$) was determined gas-volumetrically by the Scheibler method (Tatzber et al., 2007). Total organic carbon (TOC) was determined by dry combustion (Elemental Analyzer; Skalar or Shimadzu). Nutrients were determined using different extractants of increasing strength: water (P_{H2O}, K_{H2O}, Ca_{H2O}), representing easily soluble nutrients in soil solution, calcium-lactate (P_{CAL}, K_{CAL}), to consider plant-available nutrients, oxalate (P_{ox}, Al_{ox}, Fe_{ox}), for P sorbed to metal-oxides, and aqua regia (P_{tot}, Ca_{tot}, Al_{tot}, Fe_{tot}), to represent total amount of nutrients in the soil. In detail, easily soluble nutrients were extracted with deionized water at a ratio of 1:5 (w:v), shaken on a horizontal shaker for 1 h and subsequently filtered through a 0.45 μm

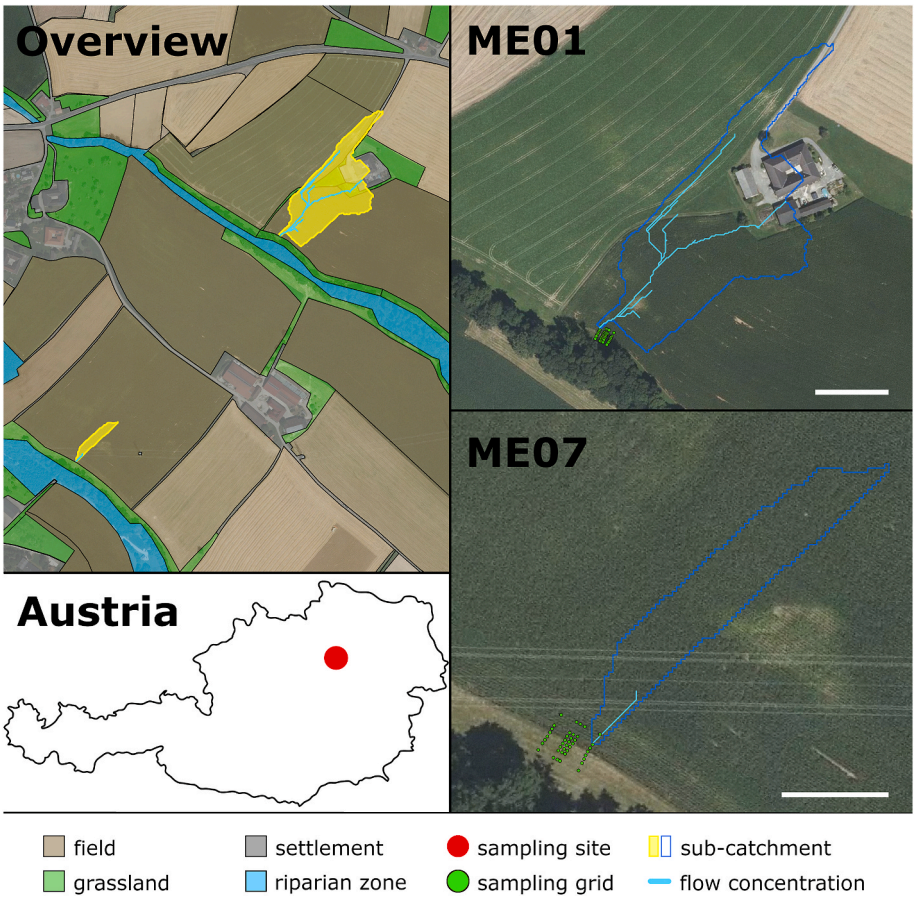

Fig. 1. Map of the sampling sites. Sub-catchments and flow concentrations were derived from a DEM (1 m resolution) and were used for the modelling. The scale bar is 50 m for ME01 and 25 m for ME07.

Table 1
Site description. Slopes derived from DEM data. Sub-catchment denotes the area that contributes to runoff and erosion above the sampling grid. Grid slope indicates the mean slope of the sampling grid alone.

Site	Sub-catchment		Flow path	VFS	Grid
	Area	Slope	Slope	Slope	Slope
ME01	1.50 ha	13.9%	8.5%	7.4%	4.8%
ME07	0.11 ha	13.2%	9.3%	3.0%	3.6%

membrane filter. Orthophosphate concentrations (P_{H2O}) were determined photometrically by the molybdenum blue method (Murphy and Riley, 1962), K_{H2O} and Ca_{H2O} were analyzed by atomic absorption spectroscopy (AAS).

Plant-available P_{CAL} and K_{CAL} were extracted based on the method described by Schüller (1969). An aliquot of dried soil was mixed with extraction solution (pH 4) consisting of 0.05 M calcium lactate, 0.05 M calcium acetate, and 0.3 M acetic acid at a ratio of 1:20 (w:v). Samples were shaken for 2 h and subsequently filtered. P_{CAL} was analyzed photometrically, and K_{CAL} by AAS as described above.

Another aliquot of soil was suspended in 0.2 M oxalate solution (pH 3: 0.11 M ammonium oxalate and 0.09 M oxalic acid; w:v = 1:50) and shaken for 4 h in the dark (Schwertmann, 1964). The extracts were then filtered and measured by ICP-OES (Optima 8300, Perkin Elmer, Germany).

Total nutrient contents (P_{tot}, Ca_{tot}, Al_{tot}, Fe_{tot}) were measured after aqua regia digestion, based on the procedure recommended by the International Organization for Standardization (ISO, 1995). Samples were digested at room temperature with a 37% HCl and 70% HNO_3 (3:1) mixture (10 ml per 1 g of soil) for 16 h. Subsequently, the suspensions were slowly warmed to 60 °C for 30 min and then to 140 °C for another hour. After cooling, 20 ml of distilled water was added, the suspensions filtered, and nutrient contents analyzed by ICP-OES.

Gravimetric soil water content and bulk density were determined after drying at 105 °C for 24 h.

2.3. P sorption and saturation indices

Two indices for soil P were determined: the Degree of Phosphorus Saturation (DPS; van der Zee and van Riemsdijk, 1988) and the Phosphor Sorption Index (PSI; Bache and Williams, 1971). The DPS is an indicator of how much P is already sorbed to available sorption sites of Fe- and Al-oxides and was calculated as:

$$DPS = \frac{P_{ox}}{\alpha \times (Fe_{ox} \times Al_{ox})} \times 100 \quad (1)$$

where α is the fraction of oxides that react with P. Following van der Zee and van Riemsdijk (1988), α was set to 0.5 (see Kleinman, 2017). The PSI is a single-point alternative to the complete sorption isotherm and, as such, an estimator for the sorption capacity of the soil (Bolster et al., 2020) and was calculated as:

$$PSI = \frac{S}{\log(C)} \quad (2)$$

where S is the sorbed concentration of P (mmol kg^{-1}) and C is the equilibrium P concentration in solution (μmol l^{-1}).

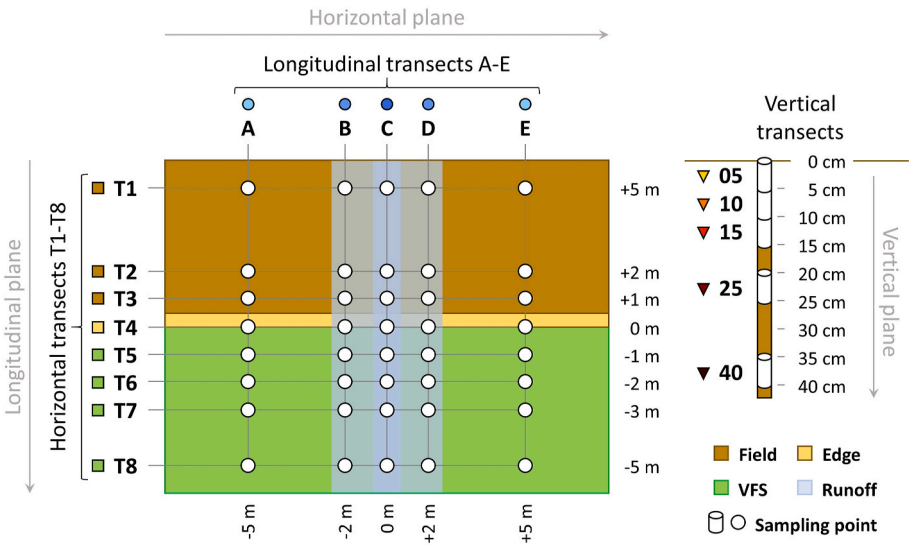

Fig. 2. Sampling design.

2.4. Statistical analysis

We produced three-dimensional depictions and boxplots for each parameter to visualize possible gradients along the transects. Further, we conducted ANOVAs for each site, using the transects as factors (+interactions) and selected parameters (P_{CAL}, DPS, PSI) as the response variables. ANOVA assumptions have been checked visually with QQ-Plots and histograms on the residuals (Figs. A3, A4), following Kozak and Piepho (2018). Dunn's post-hoc tests with Bonferroni correction were used to check for within-group differences along transects. Additionally, we conducted a principal component analysis (PCA) for each site to visualize trends along transects and corresponding parameters.

We used Python 3.9.12 embedded in Spyder 5.1.5 environment for the statistics and figure generation. Libraries used were *statsmodels* (statistics), *scipy* (assumption checking), *sklearn* (PCA), *matplotlib* (figures), *numpy* and *pandas* (data handling). Statistical significance was set at the $\alpha = 0.05$ level.

2.5. Modelling of sediment load

To find additional explanations for the measured nutrient distribution in the VFS, we simulated the sediment transport from the fields to the VFS to estimate how much sediment was eroded during the last 17 years, thus, potentially contributing to nutrient accumulation in the VFS. For this, we used the HEC-HMS model, in particular the HEC-RAS 1D Sediment Transport model (Hydrologic Engineering Center, 2022). HEC-RAS is a powerful modelling framework with various features (see https://www.hec.usace.army.mil/software/hec-ras). However we only used it to obtain coarse information about the number and severity of erosive rainfall in the investigated period to get a better estimation of the actual influence of erosion on the VFS. HEC-RAS uses a digital elevation model (DEM), soil and land use data, and precipitation as input parameters to compute infiltration and runoff volume, as well as sediment transport for single rainfall events. Rainfall data with high temporal resolution (sub-daily) was used from the rainfall station in Wieselburg, located within 5 km distance. Following a commonly used assumption about erosive rainfall (Johannsen et al., 2022), we predefined erosive rainfall events as those with a total rainfall amount of more than 10 mm rainfall or a rainfall intensity with more than 10 mm h^{-1}. The DEM was available at a resolution of 1 m. Detailed land use information was obtained at the field scale from data collected within the Integrated Administration and Control System (IACS) in the framework of the EU Common Agricultural Policy (CAP). Soil texture was measured in this study. Information on soil physical parameters and input parameters for soil modelling (erosivity, LS factor, crop factor) were taken from previous studies in the region (project ErosAT; BAW, 2023), complemented by digitally available resources (BFW, 2019).

3. Results

3.1. General remarks

Due to the high number of analyzed parameters, which are moreover examined in three dimensions, we considered it not feasible to present detailed reports for every parameter and plane. Nevertheless, we provide concise summaries for all parameters and give a detailed account of three selected parameters important for P retention: P_{CAL} as an indicator for plant-available P, PSI as an estimator for the P sorption capacity, and DPS as a proxy for P saturation (Table 2). For those three parameters, we conducted ANOVAs, which revealed a significant effect of all factors (i.e., transects) for both sites. Also, the interaction terms were mostly significant, except for *longitudinal* × *horizontal* (PSI), *longitudinal* × *vertical* (PCAL, DPS) for ME01, and *vertical* × *horizontal* (PSI) for ME07 (Table 3). Despite significant main effects, not all parameters showed distinct gradients along certain planes and also not all post-hoc tests revealed significant within-group differences (Figs. 3–5, Tables A2-4).

In the following sections, the descriptions apply for both sites, unless otherwise stated.

3.2. Modelling of sediment load

The sub-catchment that drains the field(s) above the sampling grid in the VFS (i.e., the observed sediment deposition) were 1.5 ha and 0.11 ha, with a longest flowpath length of 294 m and 97 m for ME01 and ME07, respectively. Results of the modelling with HEC-HMS suggest, that there were three and six years with erosive events for ME01 and ME07, respectively. Total sediment transport to the sub-catchment VFS over the last 17 years were 78.2 t for ME01 and 15.0 t for ME07 (Table A5). Mean standardized erosion rates (normalized to the source area) were very similar (with 10.4 and 10.3 t ha^{-1} per event) for ME01 and ME07. However, the amount of sediment that the VFSs had to deal with in the sub-catchment were different: ME01 had 5 events and a mean sediment input of 15.6 t per event, compared to ME07 with 12 events and an average of 1.1 t per event.

Table 2
Summary of most important physical and chemical parameters for each site and transect. TOC – total organic carbon; P_{H2O} – water-soluble P; P_{CAL} – CAL-soluble P; P_{tot} – total P; DPS – Degree of P saturation; PSI–P sorption index.

Gradient	Site/transect	Bulk density *[g cm-3]*	Clay *[%]*	Silt *[%]*	Sand *[%]*	TOC *[mass %]*	P_{H2O} *[mg kg-1]*	P_{CAL} *[mg kg-1]*	P_{tot} *[g kg-1]*	DPS *[%]*	PSI *[l g-1]*
Vertical	*ME_01*										
	5	1.05 ±(0.12)	31.5 ±(2.7)	62.1 ±(3.2)	6.4 ±(2.8)	2.6 ±(0.8)	5.1 ±(2.2)	64.8 ±(35.5)	0.93 ±(0.14)	10.1 ±(5.2)	5.2 ±(0.5)
	10	1.19 ±(0.10)	32.8 ±(2.5)	61.4 ±(2.3)	5.9 ±(2.0)	2.2 ±(0.3)	3.1 ±(1.6)	47.1 ±(31.5)	0.87 ±(0.14)	10.1 ±(3.4)	5.7 ±(0.8)
	15	1.20 ±(0.11)	32.2 ±(2.6)	62.1 ±(2.4)	5.6 ±(1.5)	2.2 ±(0.3)	2.8 ±(1.7)	43.9 ±(29.9)	0.86 ±(0.16)	9.9 ±(2.3)	6.0 ±(0.8)
	25	1.25 ±(0.08)	32.8 ±(2.5)	61.8 ±(1.9)	5.4 ±(1.7)	1.9 ±(0.4)	2.1 ±(1.3)	37.3 ±(30.4)	0.82 ±(0.20)	8.9 ±(3.1)	6.3 ±(1.0)
	40	1.23 ±(0.10)	32.4 ±(3.6)	64.5 ±(3.5)	3.1 ±(3.0)	1.6 ±(0.8)	0.8 ±(0.5)	8.9 ±(17.5)	0.54 ±(0.27)	5.0 ±(2.7)	6.4 ±(2.2)
	ME_07										
	5	1.08 ±(0.09)	29.5 ±(2.3)	64.9 ±(3.0)	5.7 ±(2.1)	2.9 ±(1.1)	4.7 ±(2.8)	40.7 ±(13.9)	1.02 ±(0.29)	7.0 ±(5.0)	5.7 ±(0.6)
	10	1.16 ±(0.07)	30.6 ±(3.0)	64.1 ±(3.3)	5.3 ±(1.3)	2.4 ±(0.7)	4.0 ±(1.5)	28.5 ±(13.3)	1.01 ±(0.28)	8.8 ±(2.3)	5.5 ±(0.7)
	15	1.21 ±(0.09)	30.3 ±(2.4)	64.6 ±(2.7)	5.1 ±(1.0)	2.0 ±(0.3)	2.7 ±(1.2)	24.5 ±(17.8)	0.97 ±(0.33)	8.2 ±(2.3)	5.9 ±(0.6)
	25	1.27 ±(0.09)	31.0 ±(2.8)	63.8 ±(2.8)	5.3 ±(2.4)	1.6 ±(0.3)	1.8 ±(1.7)	18.7 ±(19.2)	0.87 ±(0.30)	6.8 ±(2.8)	6.2 ±(0.8)
	40	1.37 ±(0.08)	28.7 ±(2.5)	68.0 ±(2.4)	3.3 ±(1.0)	0.7 ±(0.2)	0.1 ±(0.2)	1.3 ±(1.4)	0.74 ±(0.44)	3.5 ±(0.9)	6.1 ±(1.0)
Longitudinal	*ME_01*								0.00 ±(0.00)		
	field	1.18 ±(0.11)	32.2 ±(2.9)	61.9 ±(2.8)	5.9 ±(2.4)	2.1 ±(0.4)	3.6 ±(2.3)	64.2 ±(32.3)	0.95 ±(0.23)	11.0 ±(3.9)	6.4 ±(1.8)
	edge	1.18 ±(0.14)	32.1 ±(2.5)	61.8 ±(3.2)	6.1 ±(4.1)	1.7 ±(0.3)	3.0 ±(2.2)	49.8 ±(30.9)	0.80 ±(0.20)	9.7 ±(4.2)	5.4 ±(0.8)
	VFS	1.20 ±(0.13)	32.5 ±(2.9)	62.9 ±(2.9)	4.6 ±(1.9)	2.2 ±(0.8)	2.0 ±(1.4)	18.1 ±(19.7)	0.69 ±(0.16)	6.9 ±(2.9)	5.7 ±(0.8)
	ME_07										
	field	1.24 ±(0.12)	30.2 ±(2.8)	64.9 ±(3.3)	5.0 ±(1.1)	1.6 ±(0.5)	2.4 ±(1.7)	29.5 ±(19.2)	0.98 ±(0.33)	8.3 ±(3.3)	5.8 ±(0.8)
	edge	1.24 ±(0.15)	29.3 ±(2.7)	65.2 ±(3.8)	5.5 ±(2.1)	1.9 ±(0.8)	2.5 ±(1.9)	23.6 ±(21.0)	1.03 ±(0.36)	7.6 ±(3.5)	5.8 ±(0.8)
	VFS	1.22 ±(0.12)	30.0 ±(2.6)	65.2 ±(3.0)	4.8 ±(2.2)	2.2 ±(1.2)	2.6 ±(2.7)	14.3 ±(15.6)	0.83 ±(0.34)	5.6 ±(3.2)	6.0 ±(0.8)
Horizontal	*ME_01*										
	A	1.24 ±(0.10)	31.9 ±(2.8)	61.9 ±(2.9)	6.3 ±(3.4)	2.1 ±(0.6)	2.8 ±(2.1)	44.8 ±(37.6)	0.86 ±(0.19)	9.7 ±(4.3)	6.7 ±(1.9)
	B	1.18 ±(0.15)	31.7 ±(3.8)	63.0 ±(4.0)	5.4 ±(3.0)	2.1 ±(0.6)	3.0 ±(2.4)	43.1 ±(37.1)	0.81 ±(0.23)	9.5 ±(4.0)	5.7 ±(1.0)
	C	1.17 ±(0.12)	32.9 ±(2.2)	62.8 ±(2.0)	4.4 ±(1.8)	2.3 ±(0.8)	2.5 ±(2.0)	36.6 ±(33.6)	0.77 ±(0.25)	7.6 ±(3.9)	6.1 ±(0.8)
	D	1.19 ±(0.10)	33.5 ±(1.7)	62.2 ±(2.3)	4.4 ±(1.8)	2.1 ±(0.6)	2.3 ±(1.5)	31.5 ±(26.2)	0.79 ±(0.21)	8.1 ±(3.1)	5.9 ±(1.3)
	E	1.16 ±(0.12)	31.8 ±(2.9)	62.2 ±(3.3)	6.0 ±(2.0)	2.0 ±(0.5)	3.1 ±(2.1)	43.8 ±(34.8)	0.79 ±(0.25)	9.2 ±(4.1)	5.4 ±(0.7)
	ME_07										
	A	1.26 ±(0.13)	28.9 ±(1.8)	66.7 ±(1.6)	4.5 ±(0.6)	1.8 ±(1.0)	3.0 ±(3.2)	17.9 ±(12.5)	1.23 ±(0.26)	6.6 ±(2.9)	5.2 ±(0.5)
	B	1.23 ±(0.12)	29.4 ±(2.5)	66.2 ±(2.5)	4.4 ±(1.0)	1.9 ±(0.9)	2.3 ±(1.9)	16.5 ±(18.2)	1.14 ±(0.21)	6.3 ±(3.7)	5.9 ±(0.6)
	C	1.23 ±(0.13)	29.6 ±(2.2)	65.9 ±(2.4)	4.5 ±(1.2)	1.9 ±(1.0)	2.4 ±(2.0)	18.9 ±(17.3)	0.92 ±(0.38)	6.5 ±(3.4)	5.8 ±(0.6)
	D	1.23 ±(0.13)	30.5 ±(2.8)	64.6 ±(3.4)	4.9 ±(1.7)	1.9 ±(1.0)	2.3 ±(2.0)	20.0 ±(18.4)	0.61 ±(0.18)	6.7 ±(3.3)	5.9 ±(0.6)
	E	1.20 ±(0.12)	31.7 ±(3.2)	61.9 ±(3.5)	6.5 ±(2.9)	2.0 ±(1.0)	2.5 ±(1.9)	33.4 ±(22.9)	0.71 ±(0.21)	8.2 ±(3.7)	6.5 ±(1.0)

Table 3
ANOVA table. Results of the ANOVA for CAL-extractable P (P_{CAL}), Degree of Phosphorus Saturation (DPS), and Phosphorus Sorption Index (PSI). Asterisks indicate statistical significance of factors and interaction terms: *p < 0.05, **p < 0.01, ***p < 0.001.

Site	Factor	PCAL					DPS					PSI				
		SS	df	F	P		SS	df	F	P		SS	Df	F	P	
ME_01	Intercept	279079.2	1	1433.4	<0.001	***	15222.4	1	8086.8	<0.001	***	6415.8	1	8935.5	<0.001	***
	longitudinal	5606.5	4	7.2	<0.001	***	116.6	4	15.5	<0.001	***	50.5	4	17.6	<0.001	***
	horizontal	107243.3	7	78.7	<0.001	***	713.6	7	54.2	<0.001	***	57.8	7	11.5	<0.001	***
	vertical	50726.7	4	65.1	<0.001	***	560.4	4	74.4	<0.001	***	40.8	4	14.2	<0.001	***
	longitudinal × horizontal	13391.3	28	2.5	<0.001	***	176.9	28	3.4	<0.001	***	31.4	28	1.6	0.056	
	longitudinal × vertical	4707.5	16	1.5	0.110		41.3	16	1.4	0.172		29.9	16	2.6	0.002	**
	vertical × horizontal	15526.6	28	2.8	<0.001	***	134.6	28	2.6	<0.001	***	45.0	28	2.2	0.002	**
	Residual	20054.2	103				188.2	100				73.2	102			
ME_07	Intercept	80793.0	1	1645.1	<0.001	***	8969.4	1	10282.5	<0.001	***	6879.9	1	33996.1	<0.001	***
	longitudinal	5566.8	4	28.3	<0.001	***	66.9	4	19.2	<0.001	***	36.4	4	45.0	<0.001	***
	horizontal	9207.8	7	26.8	<0.001	***	199.0	7	32.6	<0.001	***	17.0	7	12.0	<0.001	***
	vertical	24975.8	4	127.1	<0.001	***	898.7	4	257.6	<0.001	***	12.9	4	15.9	<0.001	***
	longitudinal × horizontal	4566.5	28	3.3	<0.001	***	84.7	28	3.5	<0.001	***	12.4	28	2.2	0.002	**
	longitudinal × vertical	1819.6	16	2.3	0.006	**	40.1	16	2.9	<0.001	***	17.8	16	5.5	<0.001	***
	vertical × horizontal	9300.5	28	6.8	<0.001	***	181.3	28	7.4	<0.001	***	7.7	28	1.4	0.133	
	Residual	4812.8	98				85.5	98				22.7	112			

3.3. Physico-chemical parameters

Bulk density increased with depth but showed no discernible gradient along other planes. *Grain size distribution* did not show any conclusive patterns. However, the deepest soil layers (35–40 cm) generally had higher silt, but lower sand content. Analogously, sand accumulations along the upper left side at ME01 and along transect *E* at ME07 were at the expense of silt (Figs. A5.2, A6.2).

The pH increased with depth and was tendentially lower in the VFS than in the field. *Calcium carbonate* ($CaCO_3$) content was generally low (<1 mass %). $CaCO_3$ contents were slightly higher (up to 6%) in the VFS. The absolute and relative amount of *total organic carbon* (TOC) decreased with depth and was substantially higher in the uppermost layers in the VFS (Figs. A5.3, A6.3).

3.4. Nutrients

The overall gradients for all P and K fractions were similar (Fig. A5 & A6). Detailed results are provided for CAL-extractable P (P_{CAL}) as a representative for all P and K fractions (Fig. 3).

P_{CAL} showed clear gradients along the longitudinal and vertical transects (Fig. 3). Mean P_{CAL} decreased along the longitudinal plane, i.e., from the field to the VFS. The effect was most prominent at ME01; nevertheless, at both sites, the last two sampling points (T7+T8) were significantly distinct from the first (Figs. 4A and 5A, Table A3). No significant differences were found along the horizontal plane at ME01 (Table A4). No trends were observable at the field or edge. However, P_{CAL} showed a U-shaped distribution in the VFS at ME07 (Figs. 4D and 5D). P_{CAL} decreased with depth, and concentrations at the lowest depth (35–40 cm) were significantly lower than at the surface layer (Figs. 4B and 5B). Generally, the decrease in depth was more pronounced at the VFS, while there was substantial overlap of P_{CAL}-values of all but the lowest depth class in the field. Elevated nutrient levels were found in field samples down to the deepest sampling point at 40 cm at ME01 but not at ME07 (Figs. 4C and 5C).

The overall trend of decreasing nutrients with depth, decreasing nutrients with distance from the field edge in the VFS, as well as inconclusive gradients along the horizontal plane was also found for *water-extractable P* (P_{H2O}), *oxalate-extractable P* (P_{ox}), *total P* (P_{tot}), *water-extractable potassium* (K_{H2O}), and *CAL-extractable potassium* (K_{CAL}; Figs. A5.5, A6.5). Site ME07, however, had substantially higher P_{tot} values at transects *A* and *B*. For ME01, both K-parameters had high values at the VFS surface (higher than in the field).

Generally, *water-extractable calcium* (Ca_{H2O}) and *total calcium* (Ca_{tot}) were stable across all planes. The only discernible difference found was an increasing trend from transect *A* to *E* for Ca_{H2O} at ME07 (Figs. A5.5, A6.5).

3.5. Phosphorus indices

Oxalate-extractable aluminium (Al_{ox}) and *total aluminium* (Al_{tot}) increased tendentially with depth in the VFS at both sites and at site ME01 also in the field. Absolute differences were, however, low. No discernible gradients were found for the longitudinal and horizontal transects (Figs. A5.6, A6.6).

Mean *oxalate-extractable iron* (Fe_{ox}) concentrations were higher in the field at ME01 where they decreased until the field edge and remained stable in the VFS, while the opposite was found for ME07—stable concentrations until the field edge followed by an increase throughout the VFS (Figs. A5.7, A6.7).

Mean *total iron* (Fe_{tot}) concentrations were similar across all transects, although there was a tendency for lower concentrations (and smaller variation) at transects *D* and *E* in ME07 (Figs. A5.7, A6.7).

The *Degree of Phosphorus Saturation* (DPS) was calculated from P_{ox}, Al_{ox}, and Fe_{ox} and, therefore, showed corresponding gradients along the longitudinal and vertical transects (Fig. 3). Mean DPS decreased along the longitudinal plane, with significantly lower values at the VFS compared to field samples (Figs. 4E and 5E, Table A3). No significant differences were found for the horizontal plane. However, at the VFS a tendential U-shaped distribution was observed (Figs. 4H and 5H). The DPS decreased with depth (Figs. 4F and 5F). At ME07 differences between depth classes were more pronounced in the VFS (Fig. 5G).

The *Phosphor Sorption Index* (PSI) showed a gradient along the horizontal plane (Fig. 3). Mean PSI decreased from transect *A* to *E* at ME01, but increased at ME07, each with significant differences between the outermost transects (Figs. 4L and 5L, Table A4). Along the longitudinal plane, a significant difference was only found between *T1* and *T8* at both sites (Figs. 4I and 5I). However, at ME01, *T1* had the highest mean PSI and *T8* the lowest, which was *vice versa* for ME07. Generally, the PSI tended to increase with depth, though without statistical significance in

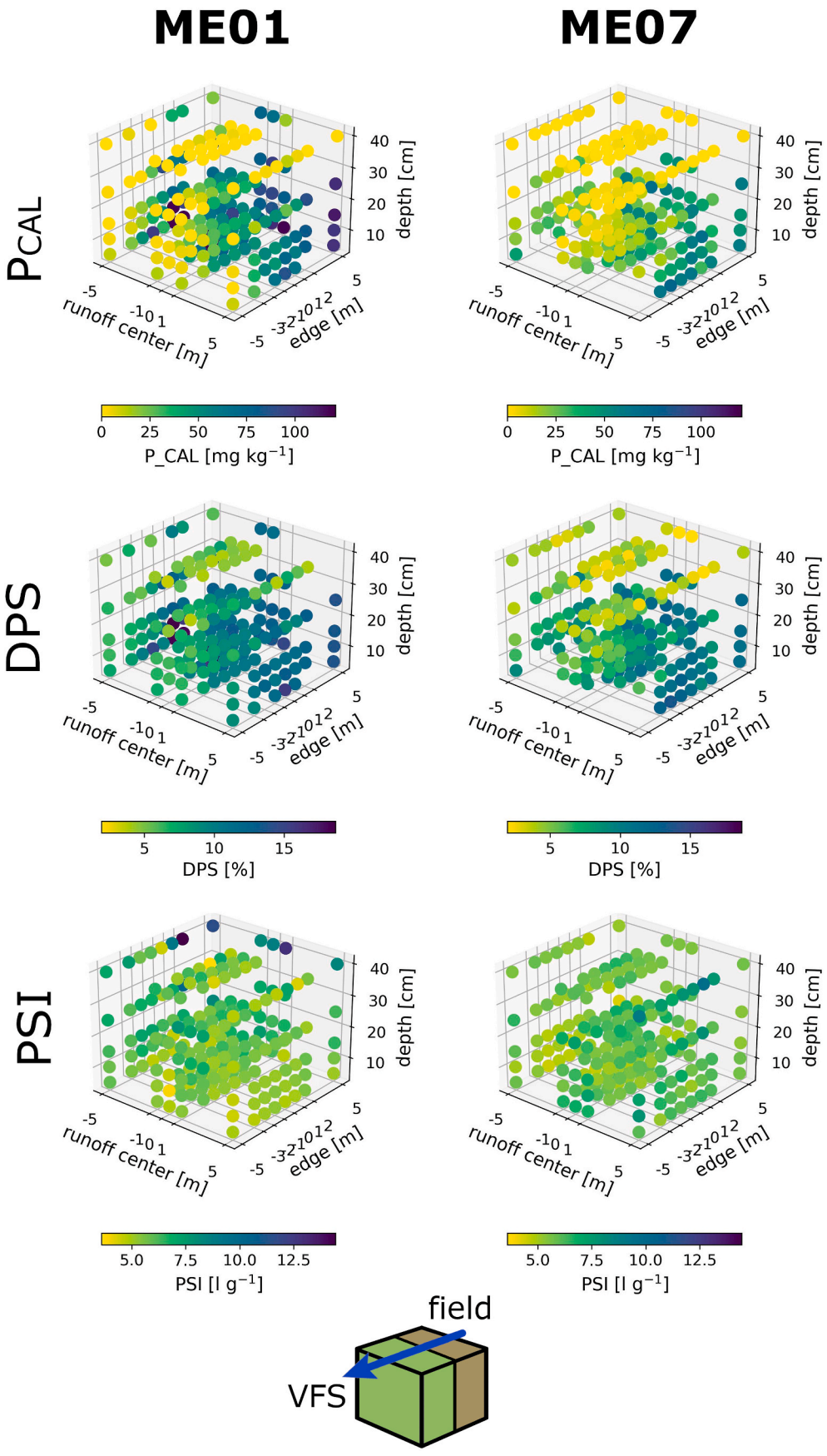

Fig. 3. Selected soil parameters in 3D. Three-dimensional distribution of CAL-extractable P [A], Degree of Phosphorus Saturation [B], and Phosphorus Sorption Index [C]. The perspective is from the VFS to field. Values are color-coded, ranging from lowest value (bright yellow) to highest value (deep purple) of the respective parameter, pooled from both sites (same color scale). The lower left axis indicates the distance from the center of runoff, the lower right axis the distance from the field-VFS edge. The insert illustrates the point of view and location of the center of concentrated runoff.

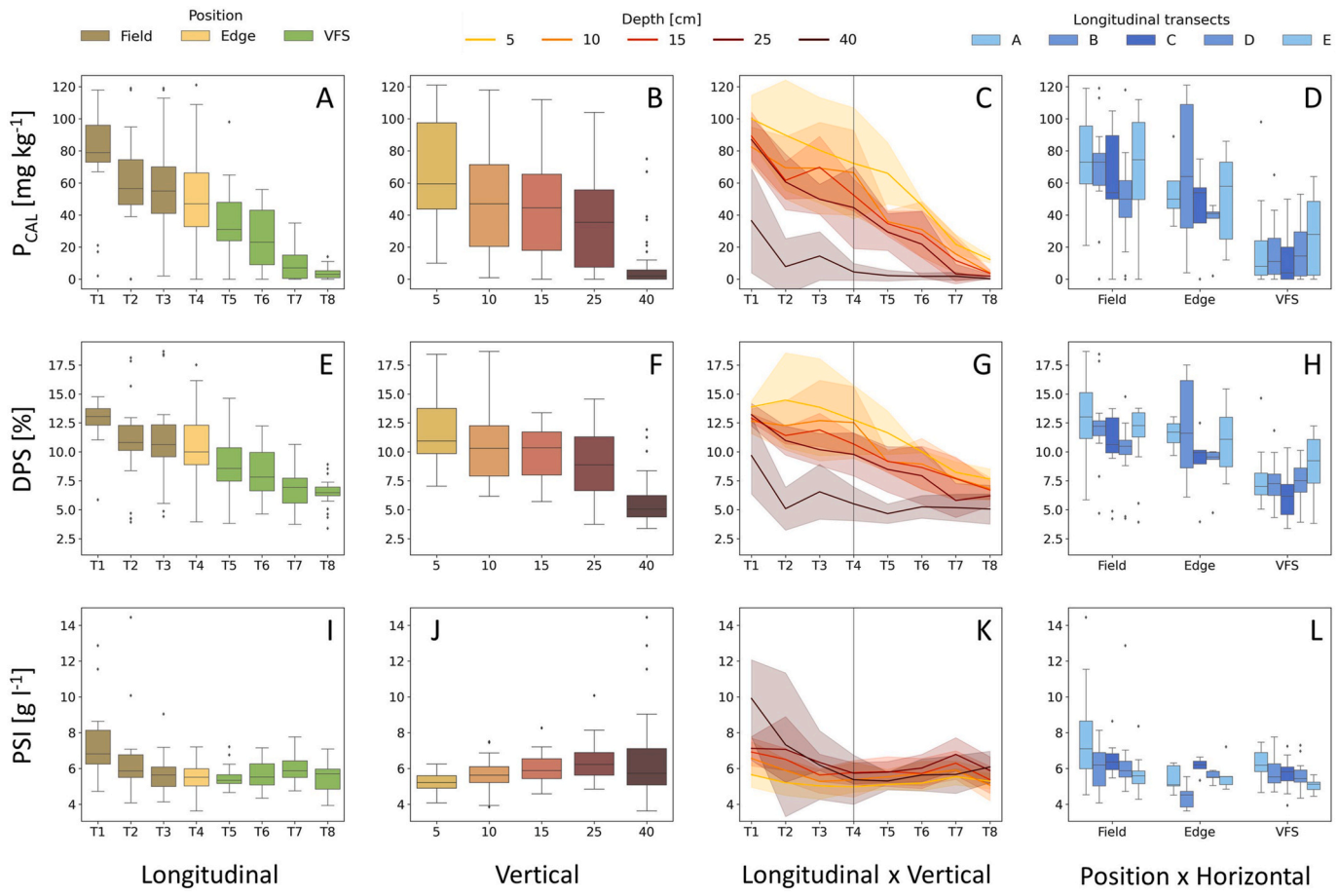

Fig. 4. Gradients of selected parameters at site ME01. Longitudinal [A, E, I], horizontal [D,H,L], and vertical [B,F,J] gradients of CAL-extractable P (P_{CAL}; top), Degree of Phosphorus Saturation (DPS; mid), and Phosphorus Sorption Index (PSI; bottom). Boxplots are pooled from all sampling points along a transect. The line graphs [C,G,K] provide a more detailed view of parameter distribution along the longitudinal plane further subdivided in depth classes (solid line – mean; shaded area – standard deviation).

ME07 (Fig. 4J–K, 5J–K).

3.6. Principal component analysis of variables and factors

The gradients described above were also reflected in the PCA (Fig. 6). For both sites, the first two principal components (PC) accounted for slightly more than 50% of the variation in the data, and all subsequent PCs accounted for 10% or less. Vertical transects (depth classes) aligned parallel to PC1 at both sites, which was associated with K- and P-parameters (especially the more easily soluble P fractions), TOC, DPS, and bulk density. The longitudinal transects were aligned parallel to PC2, associated with PSI, Ca-parameters, pH, and Fe_{ox}. The effect was mirrored between the two sites, e.g., for ME01 the PSI decreased from transect *A* to *E*, while it increased for ME07. The horizontal transects showed no linear alignment along the first two PCs but field and VFS samples could be clearly distinguished. Field and VFS samples differed regarding parameters associated with PC1 and, to a lesser extent, PC2.

4. Discussion

4.1. General

Despite long-standing research on VFS, extensive sampling schemes, such as those used in this study, are rarely applied (but see Habibiandehkordi et al., 2019, 2017; Miller et al., 2016; Sheppard et al., 2006). This lack of information may be partly due to resource limitations (funding, time, labor) and a tendency to simplify the processes involved. Often encountered, for instance, is the assumption that most P retention and cycling occurs in the uppermost few centimeters of the soil, making it obsolete to sample below the surface layer. Still prevalent are also the assumptions that VFS receive runoff water as uniform sheet flow along the entire field edge and that conditions within the VFS are homogeneous. If this were the case, one longitudinal transect would be sufficient, or multiple transects could be pooled and treated as replicates.

In this study, we looked at field-VFS transitions to check if these assumptions are justified. To this end, we applied a best-case scenario with a three-dimensional sampling array plus an extensive physical and chemical analysis. The examined sites are real-life examples that can be used as a guiding framework for future VFS research and improved sampling designs.

4.2. Modelling, rainfall, and erosion

Despite their vicinity and similarity, ME07 had substantially more erosive events than ME01, according to the HEC-HMS model. If a certain rainfall event leads to erosion depends on a multitude of factors (Lal and Elliot, 1994). One crucial aspect able to explain the differences is type of cropping. For instance, the erosive events at ME07 in 2005 and 2007 did not occur at ME01 due to the cultivation of cereals, which already had a complete soil coverage at the time when strong rainfall events occurred.

The higher total and average sediment input at ME01 was probably affected by the presence of a distinct thalweg, leading to a bundling of runoff and, consequently, higher flow velocity and erosive force. A major contributing factor was also the much smaller sub-catchment for

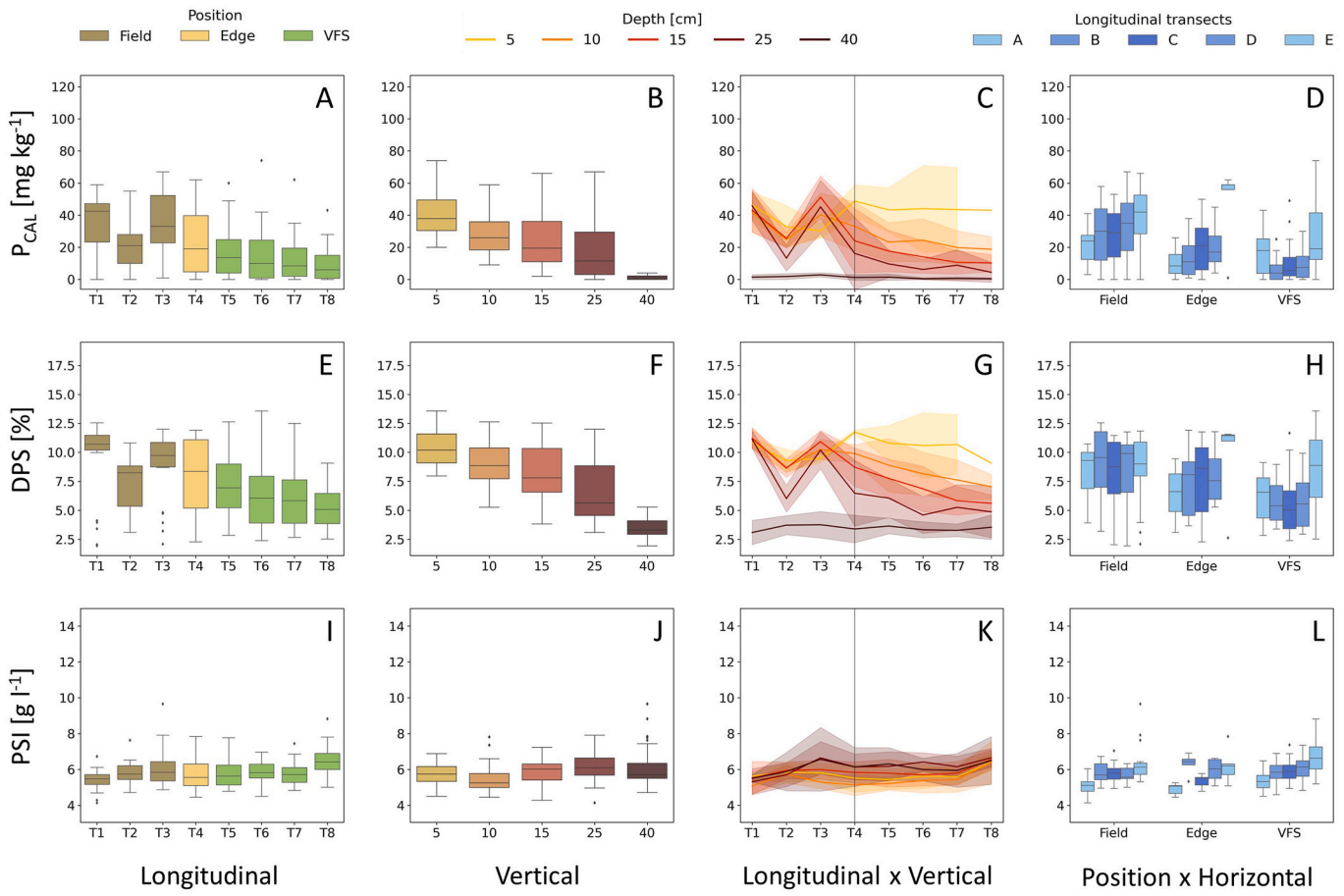

Fig. 5. Gradients of selected parameters at site ME07. See Fig. 4 for details.

ME07. While the absolute sediment transport to the VFS was much lower at ME07, the erosion per hectare would be within the same range at both sites. Nevertheless, it is the former that is crucial for VFS retention effectivity. Generally, the extent of the sub-catchments derived from DEM should be interpreted with caution because the actual extent may be different due to accumulative effects of structures smaller than the resolution of the DEM or other factors. For instance, the sub-catchment for ME01 is probably larger; the right arm of the flow accumulation appears to start within a settlement, which is, however, probably an artefact and should continue into the field above (Fig. 1). On the other hand, the left arm originates from a field to the northwest and crosses a farm track. It is likely that a non-negligible amount of runoff is discharged via this path, especially if there are pronounced tractor tracks. Consequently, the actual runoff and sediment load would be even higher.

When we compare the erosion suggested by the model with the amount of sediment that was found during our survey for sites in 2020, it appears that sediment transport was overestimated, which, however, seems to be not uncommon (Hamdan et al., 2021; Tassew et al., 2019).

Even if the magnitude of erosion may be too high, and the actual extent of the sub-catchments partly inaccurate, we are, nevertheless, confident that the timing and number of events, as well as the overall differences between sites are reliable.

4.3. Longitudinal plane: from the field to the VFS

Thirteen of 21 parameters showed a discernible gradient from *T1* to *T8* or at least pronounced differences between the field and VFS. These gradients are shaped by slope, which causes runoff generation in the first place and hence a redistribution of soil components along the flow path (Shanshan et al., 2018; Walker et al., 1968). Equally important are intrinsic factors of field and VFS soils, such as tillage or vegetation type. These entail, for instance, higher TOC contents in grasslands compared to cropland, especially near the surface (this study; Liu et al., 2016; Malhi et al., 2011, 2003).

Another vital distinction between arable fields and VFS is that the latter are usually not fertilized and, thus, should have a lower baseline nutrient content. We hypothesized that nutrients accumulate towards the edge of the field and then decrease again within the VFS due to progressive infiltration and sedimentation. A clear depletion from *T4* (field edge) to *T8* (5 m in the VFS) was evident for P_{CAL} and all other P- and K-parameters. However, we did not find an accumulation along the flow path in the field, i.e., from *T1* to *T4* at both sites. One possible explanation could be that the area close to the field edge received less direct fertilization. At any rate, a continuous accumulation of nutrients along the flow path in the field—as was found by other researchers (Habibiandehkordi et al., 2019; Stutter et al., 2009) and hypothesized by us—is not necessarily always the case. Habibiandehkordi et al. (2019) attributed their peak in P content at the field edge to the formation of a physical barrier due to tillage which caused ponding, sedimentation and a build-up of nutrients over the years. However, in a similar study, Habibiandehkordi et al. (2017) found lower field edge P contents. Apart from the barrier effect of the vegetation, there were no pronounced physical barriers at our sites.

The two VFS were similar in many respects (e.g., location, cropping, tillage, soil type, VFS vegetation), however, they showed different distributions of nutrient concentrations. At ME01, nutrient levels decreased substantially from *T4* to *T8*, while they decreased only slightly or remained stable throughout the VFS at ME07. A coherent explanation for the dissimilar behavior of the two VFS is that they had to deal with

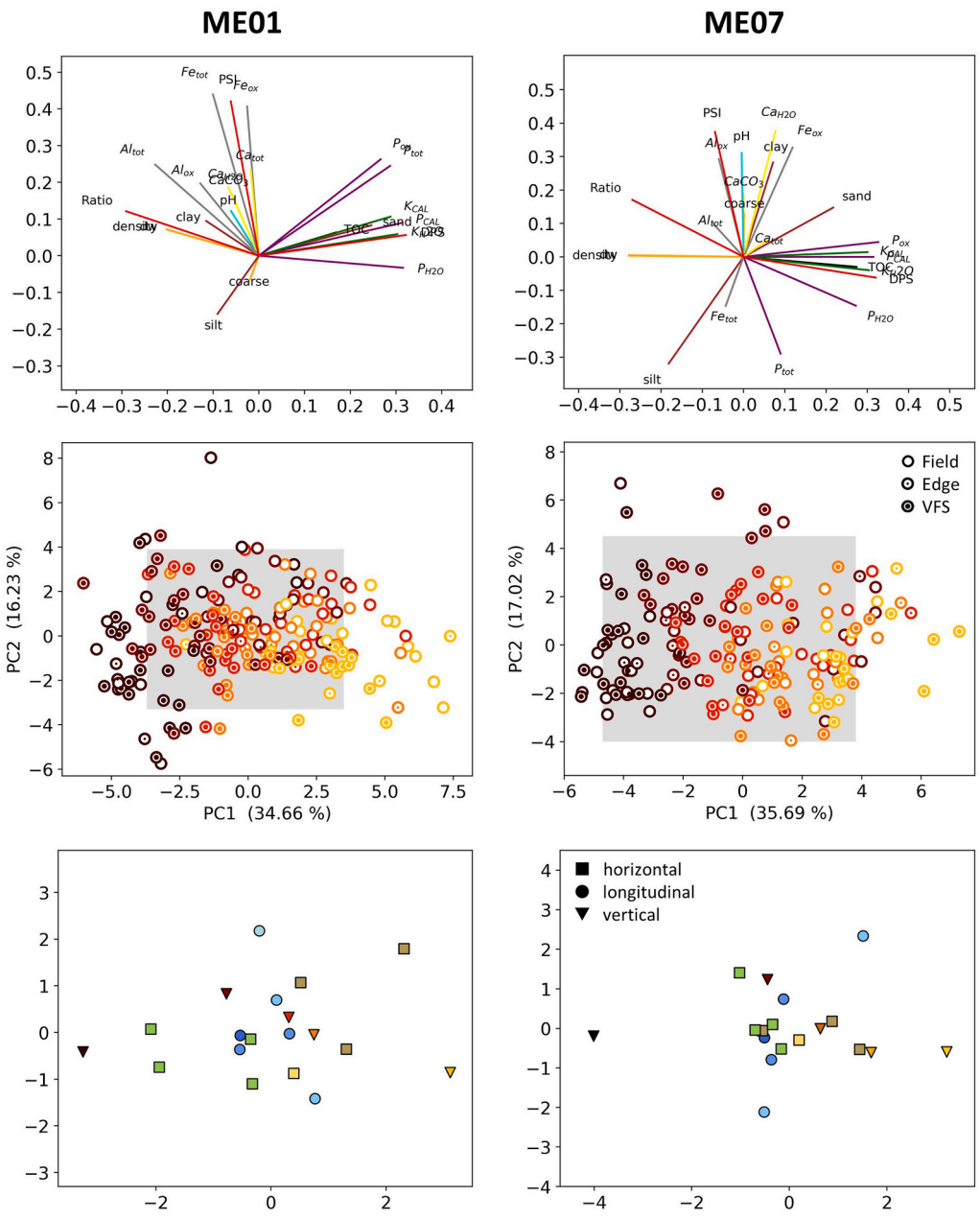

Fig. 6. Principal Component Analysis (PCA). [A] Parameter loadings. Line colors are used to distinguish parameter groups (physical, chemical, nutrients, indices, etc.). [B] PCA of all sampling points along the first two principal components. Symbols indicate position (field, edge, VFS), colors denote depth class. [C] Enlarged section of PCA (grey area in B) showing the transect means. Symbols indicate transects/planes, colors indicate individual transects. See also Figs. 2 and 4, or 5 for color coding.

different amounts of erosion. According to the HEC-HMS model, both the total sediment transport over the last 17 years, as well as the average sediment transport per erosive event were substantially higher for ME01, probably exceeding the buffer capacity of the VFS. The buffer and retention function of VFS may collapse completely under heavy runoff, for instance, once the grass stems are bent over and become submerged (Fiener and Auerswald, 2003; Haycock et al., 1997). Adapted vegetation with denser stands or stiff, robust plants could help to keep VFS functional (Blanco-Canqui et al., 2006; Kervroëdan et al., 2021). Nevertheless, deposited sediment found within the VFS demonstrated that deceleration of runoff and filtering occurred at least to some extent at both sites. Extreme events, such as the one during June 2020, require more elaborate solutions, such as retention ponds or large multizonal buffers (Stutter et al., 2020; Zak et al., 2018). The more frequent, but smaller erosive events at ME07 were better manageable by the VFS. Contrary to ME01, this lead to an accumulation of nutrients on the surface. Consequently, also the P saturation was high at the VFS surface layer, even higher than in the field. This shows that VFS—even though they are not fertilized themselves—may have equally high nutrient contents as fertilized fields due to agricultural runoff.

Apart from a few outliers, nutrient concentrations were well within the range of national soil nutrient recommendations in field (P_{CAL} 47–111 mg P kg^{-1}) and grassland areas (P_{CAL} 47–68 mg P kg^{-1}) at both sites (Baumgarten, 2022). Furthermore, the DPS was clearly below the often reported environmental threshold of 25% beyond which soils are supposed to switch to being P sources rather than sinks (Kleinman, 2017).

4.4. *Horizontal plane: from inside to outside of the flow path*

Based on the erosion patterns encountered in the VFS, our hypothesis was that nutrient concentrations would be highest along the longitudinal transect closest to the middle of the (concentrated) flow path. Consequently, we expected a symmetrical curve of nutrient content from transect *A* to *E*, with the maximum at transect *C*. For the most part, the horizontal transects had substantial overlaps and lacked statistically

significant differences. A more or less symmetrical distribution was only found for nutrients and DPS in the VFS, although with a minimum at transect *C*. This indicates removal of nutrients at the surface rather than an accumulation along the main flow path. Generally, differences were, not as evident as anticipated. Transects *A* and *E* were supposed to act as a reference, which were located outside of the concentrated flow and, thus, should not have received nutrient-enriched runoff. Still, there was substantial overlap and only few statistically significant differences, even when the data is viewed independently for the field, edge, or VFS (Table A4).

For ME01, a reason could be that the VFS was unable to effectively withhold sufficient sediment and runoff, which caused an export of nutrients and impeded an accumulation and the formation of a distinct horizontal gradient. It is also possible that the area under concentrated runoff was larger than anticipated from the extent of the observed sediment depositions in the VFS. Another explanation is that the flow path itself was not stable. While it is safe to assume that runoff convergence will always occur on the same part of the field on a larger scale (i.e., field scale, tens to hundreds of meters), for instance along a thalweg, the precise entry location of the runoff into the VFS may vary, as it is affected by several smaller-scale (i.e., meters) factors such as micro-topography, plough lines, or berms from previous sediment depositions (Hénault-Ethier et al., 2017; Shrivastav et al., 2020). These may divert runoff and force it to flow parallel to the field edge until a passage to the VFS is possible. This way, the entry location and flow path would change with each tillage or erosive event, causing the P accumulation to spread over a larger area. This blurs the area of nutrient accumulation and masks the development of a distinct gradient. The discrepancy between the modeled flow path at ME07 (indicating the flow pathway on field scale) and the middle of our sampling grid (i.e., the main flow path of an actual erosive event) likely corroborates this hypothesis (see Fig. 1). A variable runoff entry location complicates the application of countermeasures. One possible approach could be to deploy grass barriers (sensu Blanco-Canqui et al., 2006) over a wider part along the field-VFS edge so that incoming concentrated runoff is decelerated and spread no matter where exactly it enters the VFS. Another, quite contrary approach would be to force the runoff to enter at one or more specific locations (e.g., by artificial barriers) and ensure that the VFS has been adapted and reinforced accordingly at these positions. Runoff could also be collected in artificial ponds and re-distributed or filtered by biological and artificial means (Stutter et al., 2020; Zak et al., 2018). At any rate, as flow convergence can significantly diminish VFS performance, it is vital to accurately measure the area within the VFS that contributes to nutrient retention (effective area; Dosskey et al., 2002).

4.5. Vertical plane: from surface to subsurface layers

Out of 21 analyzed parameters, only four showed no vertical gradient. This was to be expected, as the physico-chemical (e.g., moisture, temperature, soil density) and biological forces (e.g., bioturbation, roots, microbial activity) that shape the soil have strong vertical aspects, governed by gravity (Phillips and Lorz, 2008). In our study, the field's uppermost three—often four—depth classes were commonly very similar due to regular ploughing and tillage that mixes and homogenizes the soil to these depths (Neidhardt et al., 2019). Usually, there is a sharp decrease of nutrients below the plough layer (e.g., Hénault-Ethier et al., 2019; Owens et al., 2008; Sharpley et al., 1993), but raised nutrient levels, significantly higher than the baseline content, may be found down to 100 cm or deeper (Kingery et al., 1994; Olson et al., 2010; Pizzeghello et al., 2014; 2016). At ME01, all nutrient parameters and indices had elevated values at the deepest sampling point in the field. This exemplifies that fertilization may lead to nutrient accumulation below the plough layer and highlights the need to include deeper soil layers to accurately study nutrient pathways. Furthermore, this shows the potential and risk of nutrient export from fields not only by surface runoff but also via leaching and interflow, which can affect surface waters and groundwater (Weihrauch and Weber, 2021). This might be the cause for elevated levels of DPS in subsurface layers of the VFS at ME01, which is also reflected in some—though not all—P- and K-parameters (Fig. 3G, A3). At ME07, nutrients did not appear to have accumulated down to 40 cm depth in the VFS. Very low nutrient contents and no or only subtle longitudinal gradients suggest that the lowest sampled depth class shows baseline nutrient levels. Generally, sub-surface layers had substantially lower DPS and higher PSI, i.e., low P concentrations and a higher capacity for P uptake. Measures that improve infiltration and divert runoff water to deeper soil layers would likely increase VFS retention effectivity and, in many cases, might be more practical and effective than increasing the VFS width.

4.6. Sampling design

Our sampling grid spanned over 100 m^2, still, it was too small to accurately depict complete nutrient gradients along all three planes. Longitudinal transects of 10 m appeared to be sufficient for ME01, but this was caused by low sediment and nutrient retention. For ME07, the transect was too short and should have extended further into the VFS. The length needed for complete nutrient retention may, however, also be beyond the actual extent of the VFS. One approach could be to link the number (or spacing) of sampling points to the width of the VFS. Samples close to the water body would give better estimates of relevant soil P concentrations and the corresponding P export potential. It should be noted, though, that stream-related issues may interfere with close-by sampling points, potentially complicating sampling (e.g., roots of riparian vegetation) and analysis (e.g., nutrient accumulation due to flooding rather than field runoff; Pankau et al., 2012). Overbank flooding severely impacts VFS performance by shortening the effective buffer width; however, this is rarely accounted for in VFS studies and designs (Sheppard et al., 2006).

The horizontal transects were probably too short compared to the area affected by runoff (shaped by average runoff width and variable entry locations), meaning that the longitudinal transects all have been within the runoff path (at one time or another). Our grid was substantially smaller than that used by Habibiandehkordi et al. (2017) and Sheppard et al. (2006), with 10 m spacing between each longitudinal transect. However, Habibiandehkordi et al. (2019) used a similar sampling scheme and did find higher nutrient contents along the central transect, suggesting that the appropriate extent is also site-specific. We recommend that future studies either increase the spacing between longitudinal transects or add sampling points at the very left and right. For specific research questions, an alternative, more flexible approach would be to sample one (or more) longitudinal transects that are definitely located within the flow path and transect(s) that are outside of it without a fixed distance.

The sampled depth classes can be considered appropriate to depict the vertical gradient of most parameters in the VFS. However, sampling deeper layers would have been necessary for the field. We recommend covering at least the plough layer (~ 30 cm) and preferably one (or more) sampling points below, especially in studies that examine both field and VFS soils.

5. Conclusions

The horizontal plane showed mostly inconclusive or U-shaped gradients in the VFS, pointing to a removal rather than an accumulation along the flow path. However, as we do not have any samples that were certainly unaffected by the runoff, we are not able to suggest to which extent nutrient concentrations were different.

Nonetheless, our results are well suited to comment on the validity of still common assumptions in VFS research (Ramler et al., 2022). Merely sampling the uppermost few centimeters of soil is likely insufficient. It is true that—quite inevitably—most nutrient retention and cycling

processes occur close to the surface. However, our results demonstrate that nutrients can reach deeper layers in relevant amounts, and, thus, should be sampled down to appropriate depths. This has potential consequences for sub-surface flow pathways and nutrient transport. The width of a VFS is an important factor contributing to retention efficacy. Equally important are, however, other VFS traits such as vegetation type and structure, as well as external factors such as field topography or the severity of erosive events. Runoff as sheet flow from the field and through the VFS is probably rare in reality and in most cases an over-simplification. Concentrated runoff was the dominant type we found in our survey for suitable sites, and we argue that flow convergence is the norm rather than the exception (see also Dosskey et al., 2002; Pankau et al., 2012). Further complicating this issue is that entry locations of concentrated runoff may vary. This strongly calls for more sophisticated sampling designs in VFS research that approach the complexity of the processes involved (e.g., spatially adapted VFS with bespoke shape, multizonal VFS, 3D buffer strips; Carstensen et al., 2020; Stutter et al., 2020). *A priori* measurements and modelling of soil P status and location of flow convergences before implementation would further contribute to ensure effective VFS designs.

Which nutrient pools should be determined is a vital decision in VFS studies and depend on the research question (Weihrauch and Opp, 2018). Our results suggest that overall trends along spatial planes were similar across the examined P- and K-fractions. Additional sites and larger sample sizes are needed to clarify the correlation of the parameters and to which degree one can be used to estimate another. Choosing the right extractant to determine the nutrient fraction most relevant to the research question remains to be important to avoid adding further noise to a challenging system.

Even though both sites were similar and close to each other, there were also significant differences that affected VFS retention. These were linked to site-specific factors, which highlights that one-type-fits-all recommendations for VFS designs are destined to fail.

In this study, we obtained a detailed—yet still incomplete—three-dimensional view of field-VFS transitions. A careful design of an appropriate sampling scheme, matching the soil's heterogeneity and the uncertainties related to flow pathways, is a vital prerequisite for any VFS study and should be given more significance. VFS can be highly valuable measures against water pollution—or fail miserably. A three-dimensional approach, comprising the longitudinal (sedimentation, nutrient export risk), horizontal (flow concentration, effective area), and vertical plane (infiltration, effective volume), appears to be indispensable for a holistic assessment of VFS.

Funding

This paper was partly funded by the Province of Lower Austria under the project RIBUST (K3-F-130/005-2019). Financial contribution was also provided by the EJP soil project "SCALE" (grant agreement no. 862695).

CRediT authorship contribution statement

David Ramler: Conceptualization, Formal analysis, Visualization, Investigation, Writing – original draft, Writing – review & editing. **Erich Inselsbacher:** Investigation, Resources, Writing – review & editing. **Peter Strauss:** Conceptualization, Resources, Supervision, Project administration, Funding acquisition, Writing – review & editing.

Declaration of competing interest

The authors declare that they have no known competing financial interests or personal relationships that could have appeared to influence the work reported in this paper.

Data availability

Data will be made available on request.

Acknowledgements

We thank Florian Darmann, Franz Aigner, Matthias Oismüller, Julia Wutzl, and Daniela Pachner for their help during field work and sample preparation. We are also grateful to Carmen Krammer for support with the modelling.

Appendix A. Supplementary data

Supplementary data to this article can be found online at https://doi.org/10.1016/j.envres.2023.116434.

References

Alewell, C., Ringeval, B., Ballabio, C., Robinson, D.A., Panagos, P., Borrelli, P., 2020. Global phosphorus shortage will be aggravated by soil erosion. Nat. Commun. 11, 4546. https://doi.org/10.1038/s41467-020-18326-7.

Bache, B.W., Williams, E.G., 1971. A phosphate sorption index for soils. J. Soil Sci. 22, 289–301. https://doi.org/10.1111/j.1365-2389.1971.tb01617.x.

Bailey, A., Deasy, C., Quinton, J., Silgram, M., Jackson, B., Stevens, C., 2013. Determining the cost of in-field mitigation options to reduce sediment and phosphorus loss. Land Use Pol. 30, 234–242. https://doi.org/10.1016/j.landusepol.2012.03.027.

Baumgarten, A. (Ed.), 2022. Richtlinie für die sachgerechte Düngung im Ackerbau und Grünland. Bundesministerium für Landwirtschaft, Regionen und Tourismus, Vienna, Austria.

BAW, 2023. ErosAT - Soil erosion in Austria [WWW Document]. Fed. Agency Water Manag. https://www.baw.at/en/wasser-boden-en/projekte/eros_at.html.

BFW, 2019. eBod - Digital Soil Map [WWW Document]. Bundesforschungszentrum für Wald. https://bodenkarte.at.

Blanco-Canqui, H., Gantzer, C.J., Anderson, S.H., 2006. Performance of grass barriers and filter strips under interrill and concentrated flow. J. Environ. Qual. 35, 1969–1974. https://doi.org/10.2134/jeq2006.0073.

Bolster, C.H., McGrath, J.M., Rosso, E., Blombäck, K., 2020. Evaluating the effectiveness of the phosphorus sorption index for estimating maximum phosphorus sorption capacity. Soil Sci. Soc. Am. J. 84, 994–1005. https://doi.org/10.1002/saj2.20078.

Carstensen, M.V., Hashemi, F., Hoffmann, C.C., Zak, D., Audet, J., Kronvang, B., 2020. Efficiency of mitigation measures targeting nutrient losses from agricultural drainage systems: a review. Ambio 49, 1820–1837.

Colloff, M.J., Pullen, K.R., Cunningham, S.A., 2010. Restoration of an ecosystem function to revegetation communities: the role of invertebrate macropores in enhancing soil water infiltration. Restor. Ecol. 18, 65–72. https://doi.org/10.1111/j.1526-100X.2010.00667.x.

Cools, N., De Vos, B., 2020. Part X: sampling and analysis of soil. In: UNECE ICP Forests Programme Coordinating Centre. Manual on Methods and Criteria for Harmonized Sampling, Assessment, Monitoring and Analysis of the Effects of Air Pollution on Forests. Thünen Institute of Forest Ecosystems, Eberswalde, Germany, p. 29 (pp + Annex).

Djodjic, F., Börling, K., Bergström, L., 2004. Phosphorus leaching in relation to soil type and soil phosphorus content. J. Environ. Qual. 33, 678–684. https://doi.org/10.2134/jeq2004.6780.

Dosskey, M.G., Helmers, M.J., Eisenhauer, D.E., Franti, T.G., Hoagland, K.D., 2002. Assessment of concentrated flow through riparian buffers. J. Soil Water Conserv. 57, 336 LP – 343.

Hydrologic Engineering Center, 2022. HEC-HMS User's Manual version 4.10 [WWW Document]. https://www.hec.usace.army.mil.

Fiener, P., Auerswald, K., 2003. Effectiveness of grassed waterways in reducing runoff and sediment delivery from agricultural watersheds. J. Environ. Qual. 32, 927–936. https://doi.org/10.2134/jeq2003.9270.

Habibiandehkordi, R., Lobb, D.A., Sheppard, S.C., Flaten, D.N., Owens, P.N., 2017. Uncertainties in vegetated buffer strip function in controlling phosphorus export from agricultural land in the Canadian prairies. Environ. Sci. Pollut. Res. 24, 18372–18382. https://doi.org/10.1007/s11356-017-9406-6.

Habibiandehkordi, R., Lobb, D.A., Owens, P.N., Flaten, D.N., 2019. Effectiveness of vegetated buffer strips in controlling legacy phosphorus exports from agricultural land. J. Environ. Qual. 48, 314–321. https://doi.org/10.2134/jeq2018.04.0129.

Hamdan, A.N., Almuktar, S., Scholz, M., 2021. Rainfall-runoff modeling using the HEC-HMS model for the Al-adhaim river catchment, northern Iraq. Hydrology. https://doi.org/10.3390/hydrology8020058.

Haycock, N.E., Pinay, G., Burt, T.P., Goulding, K.W.T., 1997. Buffer zones: current concerns and future directions. In: Haycock, N.E., Burt, T.P., Goulding, K.W.T., Pinay, G. (Eds.), Buffer Zones: Their Processes and Potential in Water Proection. Haycock Associated Limited, St. Albans, pp. 305–312.

Hénault-Ethier, L., Larocque, M., Perron, R., Wiseman, N., Labrecque, M., 2017. Hydrological heterogeneity in agricultural riparian buffer strips. J. Hydrol. 546, 276–288. https://doi.org/10.1016/j.jhydrol.2017.01.001.

Hénault-Ethier, L., Lucotte, M., Smedbol, É., Gomes, M.P., Maccario, S., Laprise, M.E.L., Perron, R., Larocque, M., Lepage, L., Juneau, P., Labrecque, M., 2019. Potential efficiency of grassy or shrub willow buffer strips against nutrient runoff from soybean and corn fields in southern quebec, Canada. J. Environ. Qual. 48, 352–361. https://doi.org/10.2134/jeq2016.10.0391.

Hille, S., Graeber, D., Kronvang, B., Rubaek, G.H., Onnen, N., Molina-Navarro, E., Baattrup-Pedersen, A., Heckrath, G.J., Stutter, M.I., 2019. Management options to reduce phosphorus leaching from vegetated buffer strips. J. Environ. Qual. 48, 322–329. https://doi.org/10.2134/jeq2018.01.0042.

Hoffmann, C.C., Kjaergaard, C., Uusi-Kämppä, J., Hansen, H.C.B., Kronvang, B., 2009. Phosphorus retention in riparian buffers: review of their efficiency. J. Environ. Qual. 38, 1942–1955. https://doi.org/10.2134/jeq2008.0087.

Hösl, R., Strauss, P., 2016. Conservation tillage practices in the alpine forelands of Austria - are they effective? Catena 137, 44–51. https://doi.org/10.1016/j.catena.2015.08.009.

Hughes, S., Reynolds, B., Bell, S.A., Gardner, C., 2000. Simple phosphorus saturation index to estimate risk of dissolved P in runoff from arable soils. Soil Use Manag. 16, 206–210. https://doi.org/10.1111/j.1475-2743.2000.tb00194.x.

ISO, 1995. Soil Quality: Extraction of Trace Elements Soluble in Aqua Regia. International Organization for Standardization, Geneva, Switzerland. ISO 11466.

Johannsen, L.L., Schmaltz, E.M., Mitrovits, O., Klik, A., Smoliner, W., Wang, S., Strauss, P., 2022. An update of the spatial and temporal variability of rainfall erosivity (R-factor) for the main agricultural production zones of Austria. Catena 215, 106305. https://doi.org/10.1016/j.catena.2022.106305.

Kervroëdan, L., Armand, R., Rey, F., Faucon, M.-P., 2021. Trait-based sediment retention and runoff control by herbaceous vegetation in agricultural catchments: a review. Land Degrad. Dev. 32, 1077–1089. https://doi.org/10.1002/ldr.3812.

Kingery, W.L., Wood, C.W., Delaney, D.P., Williams, J.C., Mullins, G.L., 1994. Impact of long-term land application of broiler litter on environmentally related soil properties. J. Environ. Qual. 23, 139–147. https://doi.org/10.2134/jeq1994.00472425002300010022x.

Kleinman, P.J.A., 2017. The persistent environmental relevance of soil phosphorus sorption saturation. Curr. Pollut. Reports 3, 141–150. https://doi.org/10.1007/s40726-017-0058-4.

Kozak, M., Piepho, H.-P., 2018. What's normal anyway? Residual plots are more telling than significance tests when checking ANOVA assumptions. J. Agron. Crop Sci. 204, 86–98. https://doi.org/10.1111/jac.12220.

Lal, R., Elliot, W.J., 1994. Erodibilty and erosivity. In: Lal, R. (Ed.), Soil Erosion Research Methods. Soil and Water Conservation Society, Ankeny, pp. 181–210.

Liu, M., Ussiri, D.A.N., Lal, R., 2016. Soil organic carbon and nitrogen fractions under different land uses and tillage practices. Commun. Soil Sci. Plant Anal. 47, 1528–1541. https://doi.org/10.1080/00103624.2016.1194993.

Malhi, S.S., Brandt, S., Gill, K.S., 2003. Cultivation and grassland type effects on light fraction and total organic C and N in a Dark Brown Chernozemic soil. Can. J. Soil Sci. 83, 145–153. https://doi.org/10.4141/S02-028.

Malhi, S.S., Nyborg, M., Goddard, T., Puurveen, D., 2011. Long-term tillage, straw and N rate effects on quantity and quality of organic C and N in a Gray Luvisol soil. Nutrient Cycl. Agroecosyst. 90, 1–20. https://doi.org/10.1007/s10705-010-9399-8.

Miller, J.J., Curtis, T., Chanasyk, D.S., Reedyk, S., Willms, W.D., 2016. Effectiveness of soil in vegetated buffers to retain nutrients and sediment transported by concentrated runoff through deep gullies. Can. J. Soil Sci. 96, 154–168. https://doi.org/10.1139/cjss-2015-0038.

Murphy, J., Riley, J.P., 1962. A modified single solution method for the determination of phosphate in natural waters. Anal. Chim. Acta 27, 31–36. https://doi.org/10.1016/S0003-2670(00)88444-5.

Neidhardt, H., Achten, F., Kern, S., Schwientek, M., Oelmann, Y., 2019. Phosphorus pool composition in soils and sediments of transitional ecotones under the influence of agriculture. J. Environ. Qual. 48, 1325. https://doi.org/10.2134/jeq2019.01.0012.

Olson, B.M., Bremer, E., McKenzie, R.H., Bennett, D.R., 2010. Phosphorus accumulation and leaching in two irrigated soils with incremental rates of cattle manure. Can. J. Soil Sci. 90, 355–362. https://doi.org/10.4141/CJSS09025.

Owens, P.N., Deeks, L.K., Wood, G.A., Betson, M.J., Lord, E.I., Davison, P.S., 2008. Variations in the depth distribution of phosphorus in soil profiles and implications for model-based catchment-scale predictions of phosphorus delivery to surface waters. J. Hydrol. 350, 317–328. https://doi.org/10.1016/j.jhydrol.2007.10.043.

Pankau, R.C., Schoonover, J.E., Williard, K.W.J., Edwards, P.J., 2012. Concentrated flow paths in riparian buffer zones of southern Illinois. Agrofor. Syst. 84, 191–205. https://doi.org/10.1007/s10457-011-9457-5.

Phillips, J.D., Lorz, C., 2008. Origins and implications of soil layering. Earth Sci. Rev. 89, 144–155. https://doi.org/10.1016/j.earscirev.2008.04.003.

Pizzeghello, D., Berti, A., Nardi, S., Morari, F., 2014. Phosphorus-related properties in the profiles of three Italian soils after long-term mineral and manure applications. Agric. Ecosyst. Environ. 189, 216–228. https://doi.org/10.1016/j.agee.2014.03.047.

Pizzeghello, D., Berti, A., Nardi, S., Morari, F., 2016. Relationship between soil test phosphorus and phosphorus release to solution in three soils after long-term mineral and manure application. Agric. Ecosyst. Environ. 233, 214–223. https://doi.org/10.1016/j.agee.2016.09.015.

Prosser, R.S., Hoekstra, P.F., Gene, S., Truman, C., White, M., Hanson, M.L., 2020. A review of the effectiveness of vegetated buffers to mitigate pesticide and nutrient transport into surface waters from agricultural areas. J. Environ. Manag. 261, 110210 https://doi.org/10.1016/j.jenvman.2020.110210.

Ramler, D., Stutter, M., Weigelhofer, G., Quinton, J.N., Hood-Nowotny, R., Strauss, P., 2022. Keeping up with phosphorus dynamics: overdue conceptual changes in vegetative filter strip research and management. Front. Environ. Sci. https://doi.org/10.3389/fenvs.2022.764333.

Roberts, W.M., Stutter, M.I., Haygarth, P.M., 2012. Phosphorus retention and remobilization in vegetated buffer strips: a review. J. Environ. Qual. 41, 389–399. https://doi.org/10.2134/jeq2010.0543.

Roberts, W.M., George, T.S., Stutter, M.I., Louro, A., Ali, M., Haygarth, P.M., 2020. Phosphorus leaching from riparian soils with differing management histories under three grass species. J. Environ. Qual. 49, 74–84. https://doi.org/10.1002/jeq2.20037.

Schindler, D.W., Carpenter, S.R., Chapra, S.C., Hecky, R.E., Orihel, D.M., 2016. Reducing phosphorus to curb lake eutrophication is a success. Environ. Sci. Technol. 50, 8923–8929. https://doi.org/10.1021/acs.est.6b02204.

Schoumans, O.F., Chardon, W.J., Bechmann, M.E., Gascuel-Odoux, C., Hofman, G., Kronvang, B., Rubæk, G.H., Ulén, B., Dorioz, J.-M., 2014. Mitigation options to reduce phosphorus losses from the agricultural sector and improve surface water quality: a review. Sci. Total Environ. 468–469, 1255–1266. https://doi.org/10.1016/j.scitotenv.2013.08.061.

Schüller, H., 1969. Die CAL-Methode, eine neue Methode zur Bestimmung des pflanzenverfügbaren Phosphaten in Böden. Zeitschrift für Pflanzenernährung und Bodenkd. 123, 48–63.

Schwertmann, U., 1964. Differenzierung der Eisenoxide des Bodens durch Extraktion mit Ammoniumoxalat-Lösung. Zeitschrift für Pflanzenernährung und Bodenkd. 105, 194–202.

Shanshan, W., Baoyang, S., Chaodong, L., Zhanbin, L., Bo, M., 2018. Runoff and soil erosion on slope cropland: a review. J. Resour. Ecol. 9, 461–470. https://doi.org/10.5814/j.issn.1674-764x.2018.05.002.

Sharpley, A.N., Smith, S.J., Bain, W.R., 1993. Nitrogen and phosphorus fate from long-term poultry litter applications to Oklahoma soils. Soil Sci. Soc. Am. J. 57, 1131–1137. https://doi.org/10.2136/sssaj1993.03615995005700040041x.

Sheppard, S.C., Sheppard, M.I., Long, J., Sanipelli, B., Tait, J., 2006. Runoff phosphorus retention in vegetated field margins on flat landscapes. Can. J. Soil Sci. 86, 871–884. https://doi.org/10.4141/S05-072.

Shrivastav, M., Mickelson, S.K., Webber, D., 2020. Using ArcGIS hydrologic modeling and LiDAR digital elevation data to evaluate surface runoff interception performance of riparian vegetative filter strip buffers in central Iowa. J. Soil Water Conserv. 75 https://doi.org/10.2489/jswc.75.1.123, 123 LP – 129.

Stoate, C., Báldi, A., Beja, P., Boatman, N.D., Herzon, I., van Doorn, A., de Snoo, G.R., Rakosy, L., Ramwell, C., 2009. Ecological impacts of early 21st century agricultural change in Europe – a review. J. Environ. Manag. 91, 22–46. https://doi.org/10.1016/j.jenvman.2009.07.005.

Stutter, M.I., Langan, S.J., Lumsdon, D.G., 2009. Vegetated buffer strips can lead to increased release of phosphorus to waters: a biogeochemical assessment of the mechanisms. Environ. Sci. Technol. 43, 1858–1863. https://doi.org/10.1021/es8030193.

Stutter, M., Wilkinson, M., Nisbet, T., 2020. 3D Buffer Strips: Designed to Deliver More for the Environment (Bristol, UK).

Stutter, M., Costa, F.B., Ó hUallacháin, D., 2021. The interactions of site-specific factors on riparian buffer effectiveness across multiple pollutants: a review. Sci. Total Environ. 798, 149238 https://doi.org/10.1016/j.scitotenv.2021.149238.

Tassew, B.G., Belete, M.A., Miegel, K., 2019. Application of HEC-HMS model for flow simulation in the lake tana basin: the case of gilgel abay catchment, upper blue nile basin, Ethiopia. Hydrology. https://doi.org/10.3390/hydrology6010021.

Tatzber, M., Stemmer, M., Spiegel, H., Katzlberger, C., Haberhauer, G., Gerzabek, M.H., 2007. An alternative method to measure carbonate in soils by FT-IR spectroscopy. Environ. Chem. Lett. 5, 9–12. https://doi.org/10.1007/s10311-006-0079-5.

Ulén, B., Bechmann, M., Fölster, J., Jarvie, H.P., Tunney, H., 2007. Agriculture as a phosphorus source for eutrophication in the north-west European countries, Norway, Sweden, United Kingdom and Ireland: a review. Soil Use Manag. 23, 5–15. https://doi.org/10.1111/j.1475-2743.2007.00115.x.

van der Zee, S.E.A.T.M., van Riemsdijk, W.H., 1988. Model for long-term phosphate reaction kinetics in soil. J. Environ. Qual. 17, 35–41. https://doi.org/10.2134/jeq1988.00472425001700010005x.

Walker, P.H., Hall, G.F., Protz, R., 1968. Relation between landform parameters and soil properties. Soil Sci. Soc. Am. J. 32, 101–104. https://doi.org/10.2136/sssaj1968.03615995003200010026x.

Wang, Y.T., Zhang, T.Q., O'Halloran, I.P., Tan, C.S., Hu, Q.C., 2016. A phosphorus sorption index and its use to estimate leaching of dissolved phosphorus from agricultural soils in Ontario. Geoderma 274, 79–87. https://doi.org/10.1016/j.geoderma.2016.04.002.

Weihrauch, C., 2019. Dynamics need space – a geospatial approach to soil phosphorus' reactions and migration. Geoderma 354, 113775. https://doi.org/10.1016/j.geoderma.2019.05.025.

Weihrauch, C., Opp, C., 2018. Ecologically relevant phosphorus pools in soils and their dynamics: the story so far. Geoderma 325, 183–194. https://doi.org/10.1016/j.geoderma.2018.02.047.

Weihrauch, C., Weber, C.J., 2021. The enrichment of phosphorus in floodplain subsoils – a case study from the Antrift catchment (Hesse, Germany). Geoderma 385, 114853. https://doi.org/10.1016/j.geoderma.2020.114853.

Zak, D., Kronvang, B., Carstensen, M.V., Hoffmann, C.C., Kjeldgaard, A., Larsen, S.E., Audet, J., Egemose, S., Jorgensen, C.A., Feuerbach, P., Gertz, F., Jensen, H.S., 2018. Nitrogen and phosphorus removal from agricultural runoff in integrated buffer zones. Environ. Sci. Technol. 52, 6508–6517. https://doi.org/10.1021/acs.est.8b01036.